Shake-Table Test of a Full-Scale 7-Story Building Slice. Phase I: Rectangular Wall

Marios Panagiotou, M.ASCE[1]; José I. Restrepo, M.ASCE[2]; and Joel P. Conte, M.ASCE[3]

Abstract: This paper is a companion to "Displacement-Based Method of Analysis for Regular Reinforced-Concrete Wall Buildings: Application to a Full-Scale 7-Story Building Slice Tested at UC–San Diego" and presents key results obtained from a full-scale 7-story reinforced concrete building slice built and tested on the George E. Brown Jr. Network for Earthquake Engineering Simulation Large Outdoor High-Performance Shake Table at the University of California, San Diego. The building was tested in two phases. This paper discusses the main test results obtained during Phase I of the experimental program. In this phase, the building had a rectangular load-bearing wall acting as the main lateral force–resisting element. The building was subjected to four historical California input ground motions, including the strong-intensity near-fault Sylmar record, which induced significant nonlinear response. The test addressed the dynamic response of the building, including the interaction between the walls, the slabs, and the gravity system as well as four issues relevant to construction optimization: (1) reduction in the longitudinal reinforcement; (2) use of a single curtain of reinforcement to transfer shear; (3) constrain of plasticity in the first level of the wall using capacity design; and (4) use of resistance-welded reinforcement in the boundary elements of the first level of the walls. The building responded very satisfactorily to the ground motions reproduced by the shake table and met all performance objectives. The effects of kinematic system overstrength and higher modes of response in the experimental response were important; this verified to a large extent the displacement-based method of analysis presented in the companion paper. **DOI: 10.1061/(ASCE)ST.1943-541X.0000332.**

CE Database subject headings: Walls; Displacement; Lateral forces; Earthquakes; Shake table tests; Concrete structures; Multi-story buildings.

Author keywords: Load-bearing walls; Displacement-based design; Capacity design; Lateral forces; Earthquakes; Shake-table testing; Three-dimensional effects; Higher-mode effects.

Introduction

This paper accompanies the paper of Panagiotou and Restrepo (2011), which discusses the displacement-based method of analysis used for this building, and presents key results of Phase I of a shake-table test program on a full-scale slice of a 7-story reinforced concrete residential building. The building slice is called "building" hereafter in this paper. The response in Phase II, which tested a T-wall, is discussed in Panagiotou et al. (2007).

The test program took place on the new Large High-Performance Outdoor Shake Table (LHPOST) funded by the National Science Foundation (NSF) through the George E. Brown Jr. Network for Earthquake Engineering Simulation (NEES) program and located at the Robert and Natalie Englekirk Structural Engineering Center of the University of California, San Diego (UCSD). During the period of October 2005 through January 2006, the building was subjected to historical southern California input ground motions that represent a range of seismic demands up to the design basis earthquake.

The test addressed the dynamic response of the building, including the interaction between the walls, the slabs, and the gravity system as well as four issues relevant to construction optimization: (1) reduction in the longitudinal reinforcement; (2) use of a single curtain of reinforcement to transfer shear; (3) constrain of plasticity in the first level of the wall using capacity design; and (4) use of resistance-welded reinforcement in the boundary elements of the first level of the walls. The companion paper (Panagiotou and Restrepo 2011) presents all the geometry and reinforcing details of the building as well as aspects related to the selection of the test structure. Lightly reinforced bearing wall buildings with wall-to-plan area ratios between 2 and 4% have performed very well during past earthquakes (Wood 1991).

Experimental Program

NEES-UCSD LHPOST

Seismic testing was performed on the unidirectional 20-MN vertical payload LHPOST. The LHPOST was built with partial funding from the NSF and is administered under the NEES. It currently operates in a single-degree-of-freedom configuration, reproducing motions in the east-west direction. Technical characteristics of the LHPOST are described by Van den Einde et al. (2004) and Ozcelik et al. (2008).

[1]Assistant Professor, Dept. of Civil and Environmental Engineering, Univ. of California Berkeley, Berkeley, CA (corresponding author). E-mail: panagiotou@berkeley.edu

[2]Professor, Dept. of Structural Engineering, Univ. of California, San Diego, La Jolla, CA.

[3]Professor, Dept. of Structural Engineering, Univ. of California, San Diego, La Jolla, CA.

Note. This manuscript was submitted on September 12, 2008; approved on September 26, 2010; published online on October 21, 2010. Discussion period open until November 1, 2011; separate discussions must be submitted for individual papers. This paper is part of the ***Journal of Structural Engineering***, Vol. 137, No. 6, June 1, 2011. ©ASCE, ISSN 0733-9445/2011/6-691–704/$25.00.

Input Ground Motions

The building was subjected to four historical earthquakes of increasing intensity recorded in southern California. Before and between earthquake shake-table tests the building was subjected to long-duration (8 min) ambient vibration tests and to long-duration (3 min) low-amplitude white-noise (WN) excitation tests. The motion of the shake table during the WN tests consisted of 0.5–25-Hz band-clipped WN acceleration processes with root-mean-square (RMS) amplitudes of 0.02, 0.03, and 0.05g. The 0.03g RMS WN tests excited the web wall beyond cracking but within the elastic limit of the reinforcement. These tests were used to identify the system (Moaveni et al. 2011) and to evaluate damage progression in the building (Moaveni et al. 2010).

The acceleration time histories as well as the elastic 5% damped acceleration and displacement response spectra of the earthquake input motions, as reproduced by the LHPOST, are shown in Fig. 1. This figure also depicts the target response spectra for immediate occupancy and for the ASCE/SEI 7-05 (ASCE 2006) design basis earthquake. It also contains the response spectra for the 3-min-long 0.03g RMS WN table motion whose intensity was low relative to the earthquake motions. The lowest-intensity input motion EQ1 consisted of the longitudinal component from the Van Nuys (VNUY) station recorded during the 1971 San Fernando earthquake ($M_w = 6.6$). The two medium-intensity input motions EQ2 and EQ3 were taken as the transverse component recorded at the VNUY station obtained during the 1971 San Fernando earthquake ($M_w = 6.6$) and the longitudinal component from the Woodland Hills Oxnard Boulevard (WHOX) station recorded during the 1994 Northridge earthquake ($M_w = 6.7$), respectively. The large-intensity input motion EQ4 corresponded to the Sylmar Olive View Med 360° recorded during the 1994 Northridge earthquake ($M_w = 6.7$).

The fundamental period of the building calculated from a linear elastic finite-element analysis assuming gross section properties for all elements and initial material stiffness properties is $T = 0.50$ s. The fundamental period of the building calculated ignoring the contribution of concrete tension stiffening along all the entire length of the web wall is $T = 1.06$ s (Panagiotou and Restrepo 2011). These two periods, which provided suitable upper and lower bounds for the fundamental period, were used to select the input ground motions. Input motion EQ1 had approximately 25% smaller spectral accelerations than the immediate-occupancy (IO) response spectrum in the period range $T = 0.5$–0.7 s (see Fig. 1). In Fig. 1, although the input motions EQ1, EQ2, and EQ3 have similar ordinates in the period interval between 0.9 and 1.1 s, the response spectrum of EQ1 is much lower than that of EQ2 and EQ3 in the period interval between 0 and 0.9 s. Input motion EQ3 is richer in high-frequency content than EQ1 and EQ2. Input motions EQ2 and EQ3 also have similar spectral ordinates in the period range of 0.5–1 s.

The response spectrum of input motion EQ4 matched the ASCE/SEI 7-05 design basis earthquake (DBE) spectrum in the period range of 0.7–1.1 s (ASCE 2006). The acceleration response spectrum EQ4 as reproduced on the LHPOST has two pronounced peaks at 0.10 and 0.31 s, respectively. The latter is caused by the ground acceleration pulse recorded at the Olive View station, whereas the former is caused by the oil-column resonance of the combined LHPOST-building system. Ground motion EQ1 adequately tested the immediate occupancy objectives of the building, which were anchored at the hazard level of 50% probability of exceedance in 50 years. Furthermore, input motion EQ4 was of higher intensity than that needed to test the life-safety performance objectives for the design basis earthquake. Motions EQ2 and EQ3 were moderate and provided important data for damage

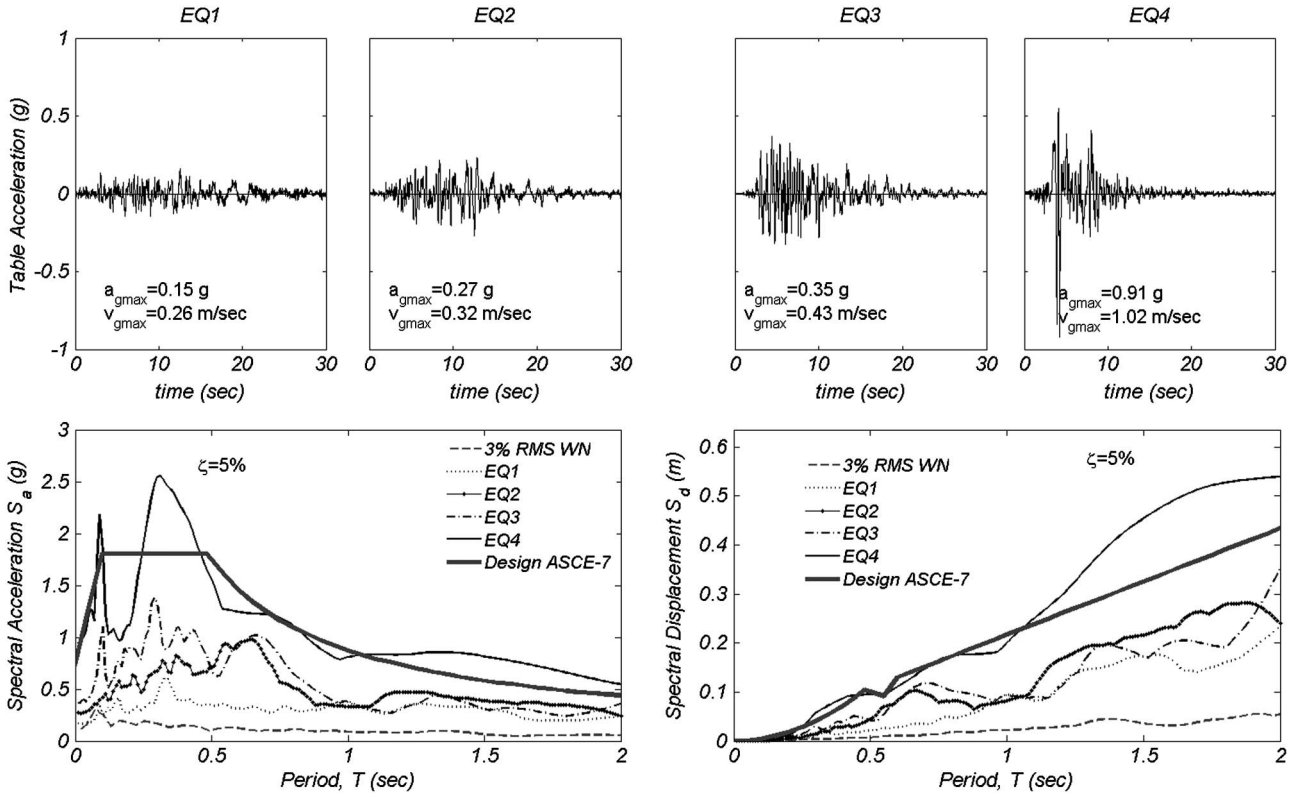

Fig. 1. Acceleration time histories and response spectra as reproduced on LHPOST

J. Struct. Eng. 2011.137:691-704.

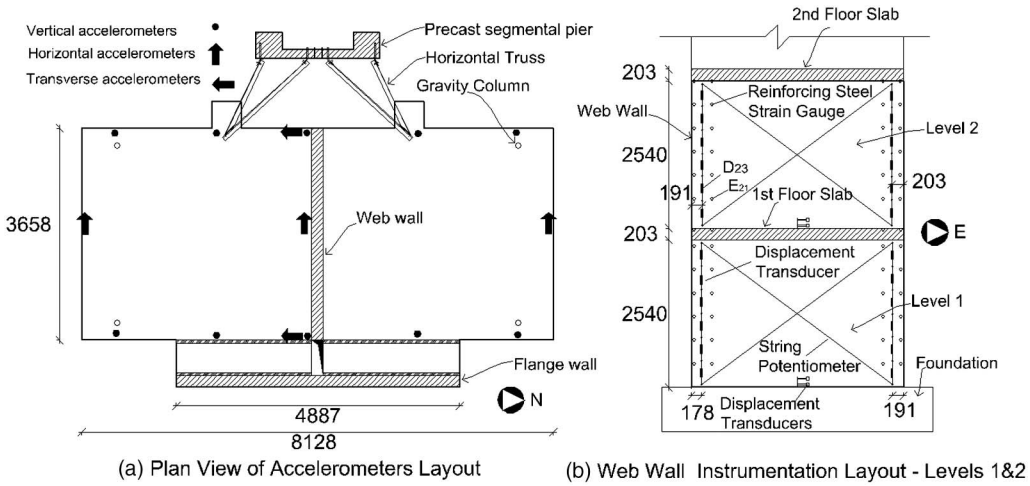

Fig. 2. (a) Plan view of locations of accelerometers and (b) elevation view of locations of displacement transducers and strain gauges on Levels 1 and 2 of web wall

progression and model calibration. These two motions did not test any specific design performance objectives.

Instrumentation

A dense array of sensors was deployed throughout the building to measure its dynamic response. It included 139 direct current (DC)–coupled single-axis accelerometers, 88 displacement transducers, and 314 strain gauges. These sensors were sampled at 240 Hz, and the sensor measurements passed through an antialiasing filter at 50 Hz. A set of seven 50-Hz, 3-mm resolution differential global positioning system (GPS) displacement sensors were deployed to measure the total lateral displacements of the building (Bock et al. 2006). Seventeen cameras recorded and broadcasted the response of different parts of the building.

Fig. 2(a) shows the horizontal and vertical accelerometers deployed on the roof. Fig. 2(b) shows the external and internal instrumentation at the first two levels of the web wall. The displacement transducers attached externally to the concrete near the edges of the web wall recorded the axial deformations near the web-wall ends, from which smeared surface strains and curvatures could be computed. Horizontal displacement transducers near the base of each level recorded sliding shear displacements. Diagonal string potentiometers recorded wall-panel shear deformations. Fig. 2(b) also shows the strain gauges placed on the reinforcing bars at Levels 1 and 2 of the web wall. String potentiometers, attached externally to the concrete, were also used at both ends of the web wall at Levels 3–7 to measure average strains. Level i in this paper refers to the portion of the building between floor slabs $i-1$ and i, where $i \geq 2$ Level 1 is that portion of the building between the foundation and the first-floor slab.

Test Results

Material Properties

The material tests performed indicated an average yield strength of the reinforcing steel of 455 MPa, a yield strength of 518 MPa for the resistance weld confining reinforcement, calculated in accordance with the 0.2% offset strain, and an average concrete compressive strength at the day of the final test of 37.9 MPa. Specific material properties are given in Panagiotou and Restrepo (2007).

General Observations

The use of four earthquake input motions with distinct features and intensities allowed monitoring of the development of different damage states in the building. Overall, the response was slightly nonlinear for EQ1, moderately nonlinear for the medium-intensity input motions EQ2 and EQ3, and highly nonlinear for input motion EQ4. Table 1 reports the peak values of relevant response parameters measured in tests EQ1–EQ4.

Fig. 3 plots the period of the building's first two longitudinal low-amplitude vibration modes identified from WN vibration test data. A fundamental period of $T = 0.51$ s was obtained from the $0.03g$ RMS WN tests at the beginning of the test program. It is close to the theoretical fundamental period of 0.50 s obtained from a three-dimensional model of the building using uncracked section properties and accepted elastic properties for concrete. The periods cited here were identified from $0.03g$ RMS WN tests. Before performing test EQ1, the fundamental period of the building had shifted to $T = 0.59$ s. This was attributable to the partial loss of tension stiffening in the concrete caused by 25 0.02 and $0.03g$ RMS WN tests performed before EQ1. After test EQ1, the fundamental period shifted to $T = 0.65$ s. After tests EQ2 and EQ3, the fundamental period increased to 0.82 and 0.88 s, respectively. The fundamental period lengthening was the result of the gradual loss of tension stiffening across the cracked concrete. Finally, after test EQ4, the fundamental period reached $T = 1.16$ s. In contrast with the first mode, the second mode period, obtained for low-amplitude vibration, only slightly changed and remained close to $T_2 = 0.1$ s (Fig. 3). Other test results clearly show the dependency of the fundamental period on the intensity of the WN tests (Moaveni et al. 2011).

A moment-curvature analysis of the web wall gives a reference yield curvature (Paulay and Priestley 1992) of the critical section $\varphi_y = 0.0034/l_w$, where l_w is the length of the web wall. Referring to the curvatures reported in Table 1, the curvature ductility (defined as the ratio of the maximum curvature to the reference yield curvature) was 3.1, 3.3, and 8.3 in tests EQ2, EQ3, and EQ4, respectively. The maximum observed curvature ductility of 8.3 is in very good agreement with the curvature ductility of 10 that is expected from the displacement-based method (Panagiotou and Restrepo 2011). In test EQ1, the maximum curvature was less than the reference yield curvature. The observed curvature ductilities confirm that the web wall exhibited limited nonlinear response

J. Struct. Eng. 2011.137:691-704.

Table 1. Peak Recorded Values of Relevant Response Parameters

Response parameter	EQ1	EQ2	EQ3	EQ4
Roof relative lateral displacement (m)	0.05	0.14	0.16	0.40
Roof residual displacement (mm)	5.6	4.3	4.3	15.5
Roof drift ratio (%)	0.28	0.75	0.83	2.06
Interstory drift ratio (%)[a]	0.35	0.89	1.03	2.36
System base moment (kN · m)	5,368	8,351	8,353	11,495
System base shear force (kN)	420	632	704	1,225
Roof acceleration (g)	0.43	0.61	0.75	1.10
Peak table acceleration (g)	0.15	0.27	0.35	0.91
Peak roof/peak table acceleration	2.9	2.3	2.1	1.2
Web-wall base curvature × wall length	0.0020	0.0107	0.0114	0.0282
Tensile chord growth (mm)[b]	7.2	24.6	27.5	64.8
Compressive chord shortening (mm) (190 mm from web-wall end)[b]	−7.2	−9.9	−6.5	−10.4
Joint shear (sliding) deformations (mm)	0.1	0.4	0.5	2.5
Longitudinal bar tensile strain (%)	0.61	1.73	1.78	2.85
Concrete compressive strain (%)	−0.07	−0.17	−0.18	−0.39
Strain rates (m/m/s × 100)	3.7	39.7	6.3	19.7

[a]Over all stories.
[b]Over the full height.

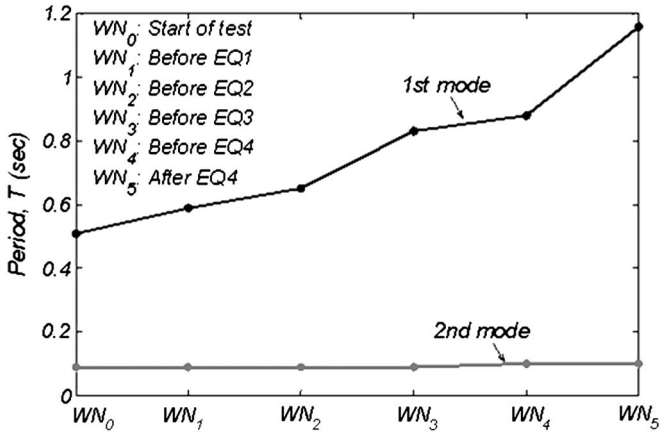

Fig. 3. Variation of period of first two longitudinal low-amplitude modes

under tests EQ2 and EQ3, whereas significant nonlinear response occurred in test EQ4.

Test EQ1 deformed the building to a maximum roof drift ratio (defined as the ratio between the maximum lateral displacement at the uppermost level and the distance of this level to the base of the wall) equal to $\Theta_r = 0.28\%$. The maximum recorded interstory drift ratio was 0.35% or $1.25\Theta_r$. This is just 8% less than the value predicted by the displacement-based design method presented in the companion paper (Panagiotou and Restrepo 2011). The tensile strain recorded in the web-wall longitudinal reinforcement at Level 1 during test EQ1 reached 0.61% or three times the yield strain. On the other hand, the compressive strain measured 50 mm from the extreme compressive fiber toward the wall axis and at 50 mm from the wall base reached −0.07% in this test. The maximum shear deformation along the construction joints was only 0.1 mm. Cracking of the wall was widespread and visible up to Level 4. Residual cracks were extremely thin and barely noticeable. The GPS sensors measured 5.6 mm of roof residual displacement. In summary, test EQ1 demonstrated that the performance objectives selected for immediate occupancy were satisfied.

The building response parameters for tests EQ2 and EQ3 were similar, although some subtle differences could be observed, especially in those response parameters sensitive to high-frequency content of the excitation. The peak roof drift ratios measured in these tests were $\Theta_r = 0.75$ and 0.83%, respectively. Recorded interstory drift ratios in these tests were 1.19 and 1.24 of their respective roof drift ratios. At the base of the wall, moderate yielding occurred in the web-walls longitudinal reinforcement, which reached a tensile strain of 1.73 and 1.78%, respectively. The concrete compressive strain measured near the extreme compressive fiber at the base of the wall reached −0.17 and −0.18% in tests EQ2 and EQ3, respectively. Yielding took place also in the extreme longitudinal reinforcement of the web wall at the base of Level 2 in tests EQ2 and EQ3. Measured tensile strains at these two tests in Level 2 reached 0.36 and 0.39% on the west and east sides of the wall, respectively. In both tests, tensile strains in the extreme longitudinal reinforcement in Level 3 were very close to the yield strain. In these tests, the maximum shear deformation along the construction joints was 0.4 and 0.5 mm, respectively. The roof residual displacements were 4.3 mm in both tests EQ2 and EQ3. The highest strain rate in the longitudinal reinforcement was measured during test EQ2 (see Table 1). This was caused by the first spread of the Lüders bands into the gauged portion of the bars during this test. This level of strain rate resulted in a 7% increase of the steel yield strength during test EQ2, according to coupons tested under strain controlled conditions in a universal testing machine to the same strain rate and strain history (Panagiotou and Restrepo 2007).

In test EQ4, the maximum roof drift and interstory drift ratios were 2.06 and 2.36%, respectively, with a maximum interstory drift ratio of $1.15\Theta_r$. A comparison of the ratios between the maximum interstory drift and roof drift ratios in tests EQ1 to EQ4 shows a consistent reduction as the testing progressed. This is also manifested in the development of localized plasticity at the base of the wall, which increased as the displacement demand in the tests increased. In this test, the tensile strain in the longitudinal reinforcement in the plastic hinge at the base of the wall reached 2.85%, and the concrete strain near the extreme compressive fiber reached −0.39%. This strain level is in the accepted range of strains; spalling of the concrete cover was observed. The weld resistance

confinement grids provided excellent lateral stability to the reinforcing bars once the concrete cover spalled off because no evidence of longitudinal bar buckling was observed at the end of Phase I testing. Significant yielding in the longitudinal reinforcing bars occurred at level 2, with the maximum measured tensile strain to reach 0.88 and 1.95% on the east and west side of the web wall, respectively. This is in general agreement with the analysis (Panagiotou and Restrepo 2011) which predicted that both sides of the wall at Level 2, and especially the west side, would experience yielding. Levels 3 and 4 yielded also solely on the west side, with the maximum tensile strain to reach 0.25 and 0.28%, respectively. This also verifies the analysis results that indicated the possibility of yielding on the west side of the wall at Level 4.

The maximum shear deformation along the construction joints reached the small value of 2.5 mm. Test EQ4 ended with a surprise lap-splice failure at the west end of the web wall at the base of Level 2. This lap splice survived unscathed the peak demand but degraded afterward. This lap-splice failure was manifested by a large split crack extending one-third of the height of the second level. In addition to splitting of the concrete in this region, residual crack widths of approximately 1.3 mm were observed. The roof residual lateral displacement recorded after this test was only 15.5 mm.

Fig. 4(a) shows the flexure-shear crack pattern observed on the web wall at Level 1 after test EQ4. Figs. 4(b) and 4(c) depict the west side of the web wall at Levels 1 and 2 after test EQ4. The limited spalling of the concrete cover at the base of the web wall is shown in Fig. 4(b). Fig. 4(c) shows the split vertical crack that developed from the lap-splice failure at the west end on Level 2.

For the seismic tests performed, the single curtain of wall reinforcement resulted in excellent behavior. In spite of the thin aspect ratio of the web wall, no out-of-plane related stability deformations were measured. In summary, according to observed/measured damage, the building survived test EQ4, corresponding to the design basis earthquake, with limited damage. The building did not present obvious life-safety hazards. The building might not be immediately operational, but would require only minimum repairs. Furthermore, maximum strains and roof drift ratios in test EQ4 were smaller than those limits set to meet the life-safety performance objectives in the displacement-based design method described in the companion paper (Panagiotou and Restrepo 2011).

Hysteretic Response

Fig. 5 shows the building system base overturning moment versus roof lateral relative displacement hysteretic response for tests EQ1–EQ4. Positive displacement is defined toward west. The building system base overturning moment was estimated as the sum over all floors of the product of the tributary seismic mass, the total floor acceleration, and the floor height over the base of the wall. The base overturning moment also accounts for the small P-Δ effects as well as for the small mass rotatory inertia effects.

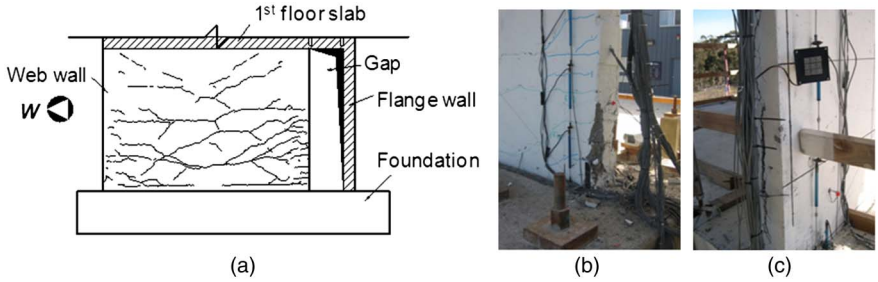

Fig. 4. Observed damage of web wall after test EQ4: (a) south side view of web wall—Level 1; (b) west bottom end of web wall at Level 1; (c) west bottom end of web wall above first-floor slab

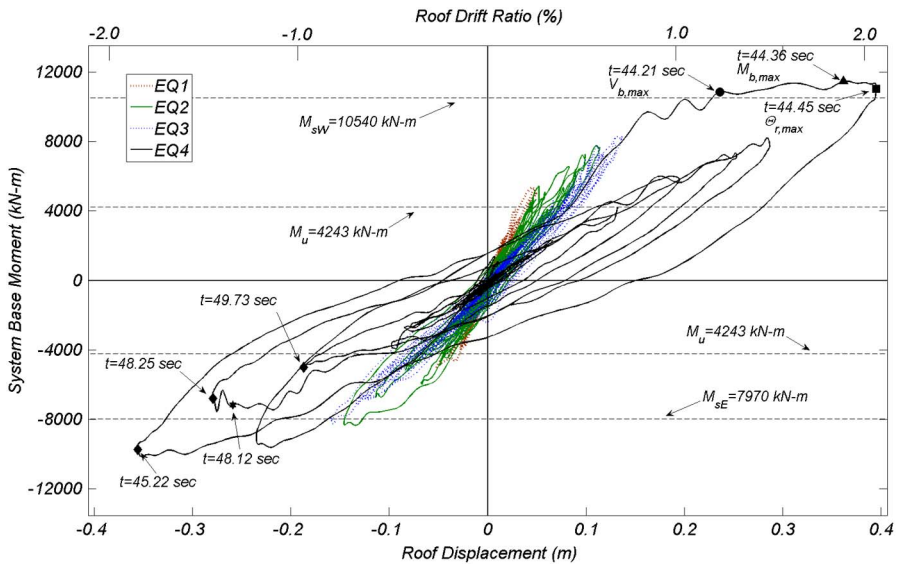

Fig. 5. Building system base overturning moment versus roof relative lateral displacement

J. Struct. Eng. 2011.137:691-704.

The total floor acceleration was calculated as the average of the three horizontal accelerometers at each floor [see Fig. 2(a)]. Lateral displacements were calculated from the accelerations measured by the three horizontal accelerometers at every floor by using filtering and double integration of the measured acceleration. A high-order (5,000), 0.2–25 Hz band-pass, finite impulse response (FIR) filter was used in Matlab (*Matlab Reference Guide* 2008). The calculated displacement time histories were in excellent agreement with those measured directly with the GPS displacement sensors in the test program (Bock et al. 2006; Panagiotou 2008). Fig. 5 also shows the web-wall design base moment, M_u, as well as the maximum system base moments M_{sE} and M_{sW} for eastward and westward response, respectively, calculated with the displacement-based method of analysis (Panagiotou and Restrepo 2011). Very good agreement is observed between the estimated and measured system base overturning moment for the westward response. The method of analysis did not consider the small bending moment carried by the flange wall and did not account for the strain-aging effects that played a role for eastward response. Strain aging occurs in certain types of steel after undergoing plastic deformations when soluble nitrogen diffuses through free dislocations in the steel structure and pins them, changing its mechanical properties and rising the yield strength upon time (Restrepo-Posada et al. 1994). The lapse between tests EQ3 and EQ4 was 55 days, sufficient for the development of some strain aging. Rebar test coupons were subjected to the same strain rate and strain history and were tested with and without the lapse between tests for EQ3 and EQ4 (Panagiotou and Restrepo 2007). These tests indicate that strain aging contributed to an increase of 7% of the flexural strength of the web wall for eastward response.

The system total base shear force versus roof lateral displacement hysteretic response is plotted in Fig. 6. This figure also shows the design base shear force (V_u) and the eastward (V_{sE}) and westward (V_{sW}) system base shear forces, including section and kinematic system overstrength, as well as second-mode effects computed from the displacement-based design method (Panagiotou and Restrepo 2011). Excellent agreement is observed between maximum measured and predicted base shear forces for both directions of the response. Such good agreement is merely a coincidence as will be explained in the section "Response Envelopes."

Comparison of the system base overturning moment and total base shear force hysteretic responses shows (1) significant system overstrength and (2) erratic loop traces in the base total shear force hysteretic response when compared to the loops observed from the base moment hysteretic response. The base moment overstrength factor calculated as the ratio of the maximum measured system base overturning moment and design base overturning moment of the web wall only was $\Omega_{oM} = 2.71$. The observed system base moment overstrength is attributable to (1) section flexural overstrength and (2) kinematic system overstrength. These two sources of overstrength will be examined in detail in the following sections. The base shear overstrength factor calculated as the ratio of the maximum measured system base shear force and the design base shear force of the web wall only was $\Omega_{oV} = 4.20$. The difference in magnitude between Ω_{oM} and Ω_{oV} is attributable to the higher modes in the response of the building. The influence of the higher modes will also be discussed in the following.

Fig. 7 plots the disaggregation of the main sources of deformation contributing to the peak measured roof lateral relative displacement for tests EQ1–EQ4. Four sources of deformations are considered. The first is the combined shake-table platen-hydraulic bearings-foundation-soil deformation, termed in this figure as the *substructure*. The second is the localized rotation manifested at the

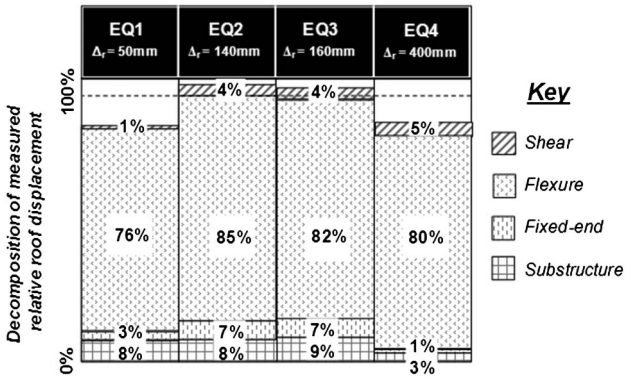

Fig. 7. Contribution of four different sources of deformation to peak roof relative lateral displacement

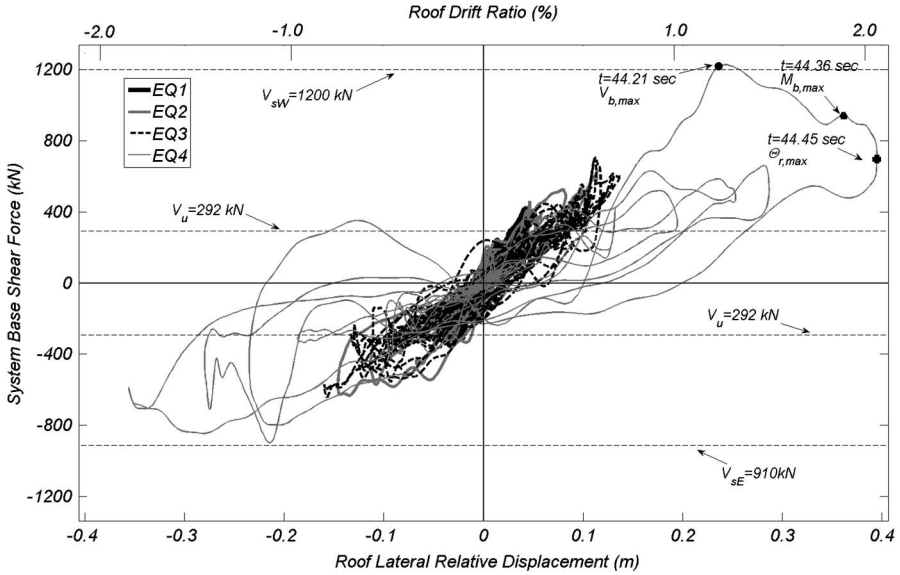

Fig. 6. Building system base shear force versus roof relative lateral displacement

J. Struct. Eng. 2011.137:691-704.

base of the web wall (the fixed end) which is caused by bar bond slip of the wall longitudinal reinforcing bars anchored in the foundation. The third is the flexural deformation of the web wall. Fourth is the shear deformation measured at the first two levels of the web wall. The lateral displacements contributed by these four sources are normalized in Fig. 7 by the peak roof lateral displacement recorded in each of the tests. Fig. 7 shows that the sum of the displacements is within 88% of the peak roof lateral displacements, indicating excellent disposition of the instrumentation. This figure shows that the wall responded primarily in flexure, which contributed to approximately 80% of the roof lateral displacement. The same calculations were repeated to obtain the contribution of the different sources of deformation to the roof lateral displacement when the peak shear force was recorded in each of the tests. The results varied only slightly from those plotted in Fig. 7.

Section Flexural Overstrength

The maximum curvature attained in the plastic hinge that developed in the web wall during test EQ4 was 7.72×10^{-3} rad/m, which corresponds to a curvature ductility of 8.3. The theoretical flexural strength at this curvature is $6,369$ kN · m for an axial compressive force of $N = 809$ kN. Therefore, the theoretical section flexural overstrength (defined as the ratio of the flexural strength to the design web-wall moment) was $\Omega_{os} = 1.50$. This overstrength factor was chiefly the result of the strength reduction factor used in this design, e.g., actual yield strength of reinforcing steel larger than nominal/specified yield strength used in design, resulting in an excess of web-wall longitudinal reinforcement. The value obtained for Ω_{os} is well within the expected range of values.

Kinematic System Overstrength

Kinematic overstrength is defined here as the increase in resistance caused by the interaction between the cantilever web wall and those elements framing into it. The theoretical estimation of this system effect for the building is presented in the companion paper by Panagiotou and Restrepo (2011).

A source of kinematic overstrength in the building was the warping and bending of the slabs caused by the deformation of the web wall (i.e., lengthening of tensile chord and shortening of compressive chord). The slabs warped and bent because of the restraints imposed by the gravity columns [see Figs. 8(a) and 8(b)]. Table 1 reports the elongation and shortening of the tensile and compressive chords of the web wall during the seismic tests. During test EQ4, the tensile chord lengthened by 65 mm over the entire height of the wall. This value is 38% greater than the expected growth of 47 mm (Panagiotou and Restrepo 2011)

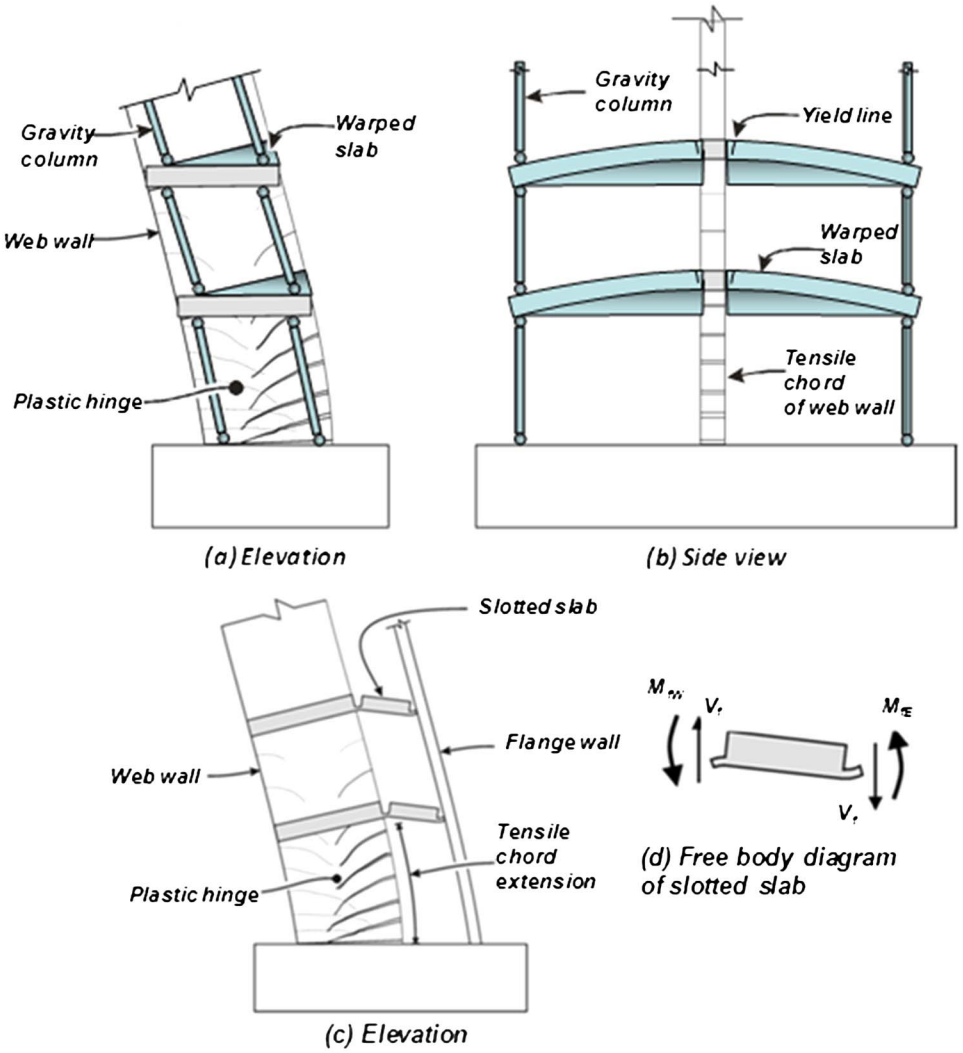

Fig. 8. Exaggerated deformed shape explaining kinematic overstrength caused by (a) and (b) coupling of wall, slabs, and gravity columns and (c) and (d) slotted slab

J. Struct. Eng. 2011.137:691-704.

because the expected growth was calculated considering only for the elongation in the plastic-hinge region. This growth caused significant tension and additional compression forces in the gravity columns. In test EQ4, the maximum moment resisted by the first-level gravity columns, which had been instrumented with strain gauges, represents 12% of the maximum measured system base overturning moment and 33% of the web-wall design moment M_u.

Another source of kinematic overstrength was the slotted slabs between the web and flange walls. Elongation and shortening of the east chord of the web wall occurred for westward and eastward displacement responses, respectively. Such change in length was negligible in the flange wall because of the small level of strains that developed. Thus, each slotted slab was forced to rotate and develop positive and negative yield lines along the slots [see Figs. 8(c) and 8(d)]. The negative and positive moment capacity along the yield lines at various floors next to the flange wall was $M_{f\mathrm{E}} = 6.2\ \mathrm{kN \cdot m/m}$, whereas the moment capacity on the yield lines next to the web wall was $M_{f\mathrm{W}} = 10.2\ \mathrm{kN \cdot m/m}$. The axial forces that developed in the slotted slabs because of the flange wall inertial mass had minor influence on the previously mentioned moment capacities.

The flexural capacity and the corresponding shear forces that developed per unit length along the yield lines were small; however, the total shear force that developed along each yield line was not negligible because of the significantly small width of the slots. Accumulation of the shear forces over the seven floors caused an axial force at the east edge of the web wall and at the west edge of the flange wall equal to $N_f = 921$ kN. For westward response, this force increased the axial compressive load in the web wall, whereas it decreased it for eastward response (Panagiotou and Restrepo 2011). The variation N_f of the axial force in the flange wall and the web wall caused an increase of the system moment resistance at the base of approximately 3,658 and 946 $\mathrm{kN \cdot m}$ for westward and eastward response, respectively. Such increase in resistance overturning moment represents 32 and 9% of the maximum measured system base moment for westward and eastward displacement response, respectively. They also represent 90 and 22% of the design moment M_u. The aforementioned results and discussion are based on unidirectional flexural behavior of the slotted connections and zero axial force in the slotted slab. A more accurate assessment of the effect of the slotted slabs should consider all three components of the flexural behavior (bending in the longitudinal and transverse directions in addition to warping), as well as the variation of the axial force in the slotted slabs.

Decomposition of the system base moment resistance for westward response demonstrates that (1) the base moment capacity of the web wall corresponded to 55% of the maximum base system moment recorded in test EQ4; (2) coupling of the web and the flange walls through the slotted slabs contributed 32%; (3) 10% was carried by the pairs of gravity columns; (4) the base moment capacity of the two transverse walls contributed 2.5%; and (5) the rotatory inertia forces contributed 0.5%. An increase of the system base moment caused by the kinematic system overstrength previously described resulted in an even larger increase of the shear force demand on the web wall (Panagiotou and Restrepo 2011).

Any direct extrapolation of the kinematic interaction observed in this test to general buildings may be inappropriate. The presence of gravity columns at such close locations to walls is not common in actual buildings. However, there are cases in which such columns are near walls. In any case, a first-order analysis, as commonly performed in engineering practice, can provide the compression and tension axial forces that these columns will carry

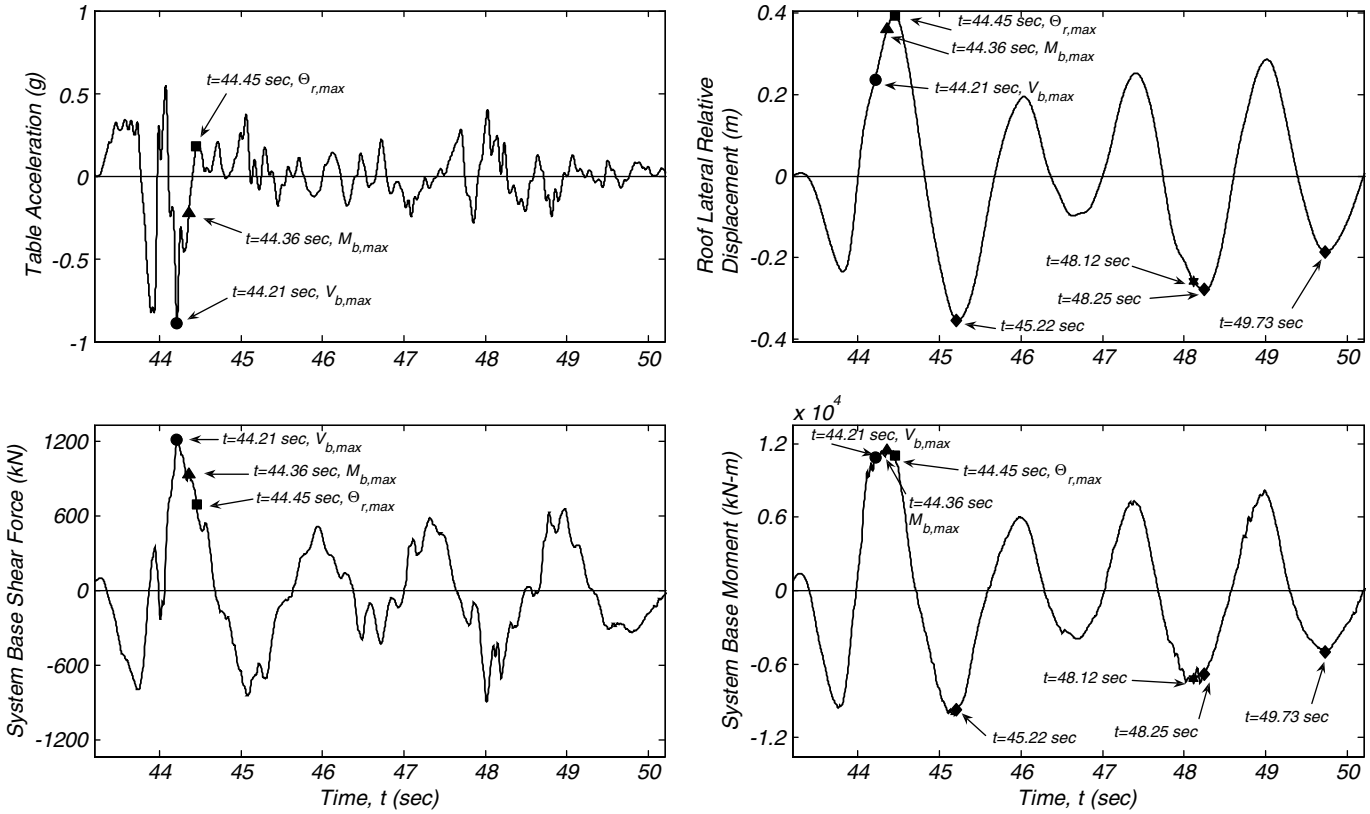

Fig. 9. EQ4—time histories between $t = 43.2$ and 50.2 s of (a) table acceleration, (b) roof relative lateral displacement, (c) system base shear force, and (d) system base moment

J. Struct. Eng. 2011.137:691-704.

during seismic response. Another point is that the coupling effect of the slab may be significantly greater in real buildings because the slabs were deliberately slotted in the present building.

Higher-Mode Effects

Previous sections dealt with sources of overstrength that can be predicted through static analysis of a well-conceived analytical model of the building. However, some response quantities are affected by the building's dynamic behavior. In particular, higher-mode effects can play a significant role on the dynamic response (Park and Paulay 1975).

Figs. 9(a) and 9(d) show the time histories of table acceleration, roof relative displacement, system total base shear force, and system base overturning moment for test EQ4 to be between $t = 43.2$ and 50.2 s, respectively. Peak responses occurred during this time bracket. For example, the peak total system base shear force ($V_{b,\max}$) occurred at $t = 44.21$ s, the peak system base overturning moment ($M_{b,\max}$) occurred at $t = 44.36$ s, and the peak roof drift ratio ($\Theta_{r,\max}$) was recorded at $t = 44.45$ s. Also, the lap-splice failure initiated at $t = 48.12$ s, and the maximum strain on the second level after the lap splice failed was recorded at $t = 48.25$ s. All these events are also indicated in the system base overturning moment and system total base shear force hysteretic responses depicted in Figs. 5 and 6, respectively.

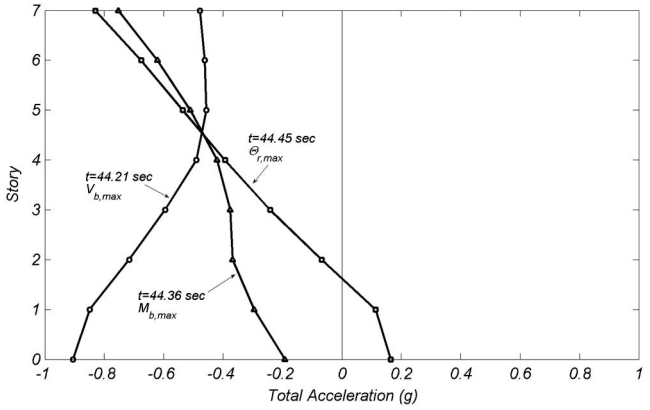

Fig. 10. Total acceleration profile at characteristic instants of time during test EQ4

In test EQ4, the peak table acceleration ($a_{g,\max}$) and the system maximum base shear force ($V_{b,\max}$) occurred at $t = 44.21$ s. The peak ground acceleration in this motion is the result of a local high-frequency pulse of $0.5g$ amplitude and 0.09-s duration. The period and amplitude of this local acceleration pulse affects the seismic excitation and contributes to the response of the higher modes, especially the second mode, which had a period of 0.1 s. The total acceleration profile along the height of the building at $t = 44.21$ s, plotted in Fig. 10, is significantly affected by the higher modes of response, especially of the second mode. The resultant lateral force at $t = 44.21$ s is located at 46% of the height of the building, as it will be examined in the following. Fig. 10 also shows the measured horizontal acceleration profiles at the occurrence times of $M_{b,\max}$ and $\Theta_{r,\max}$. These two profiles have a more linear shape. The three acceleration profiles intersect between Levels 4 and 5. This intersection point corresponds to the nodal point of the second mode shape. The acceleration profiles below this point are more or less linear (i.e., given by a straight line between acceleration of nodal point and table acceleration).

Fig. 11 plots the vertical position of the resultant lateral force in tests EQ1–EQ4 and in two WN tests versus the base shear coefficient. The position was computed as the ratio of the measured system overturning base moment to the total system base shear force at a given sampling time. In this figure, the lateral force position is presented as a ratio of the building height measured from the top of the foundation. The points plotted in Fig. 11 are for those sampling times when the system base overturning moment exceeded 90% of the peak system base overturning moment measured in each test. Furthermore, Fig. 11 also shows the nondimensional ratios $M_u/(V_u H)$ and $M_{sW}/(V_{sw} H)$. Ratio $M_u/(V_u H)$ is the normalized location of the first-mode lateral force in the displacement-based design method described in the companion paper. Ratio $M_{sW}/(V_{sw} H)$ is the normalized location of the maximum westward base shear force calculated from the displacement-based design method, assuming that it occurs concurrently with the maximum westward system overturning moment.

Low-amplitude white-noise tests WN1 and WN4 were performed before EQ1 and before EQ4, respectively. Note in Fig. 11 that in tests WN1, WN4, and EQ1, when the building had limited nonlinear response, the location of the resultant lateral force varied

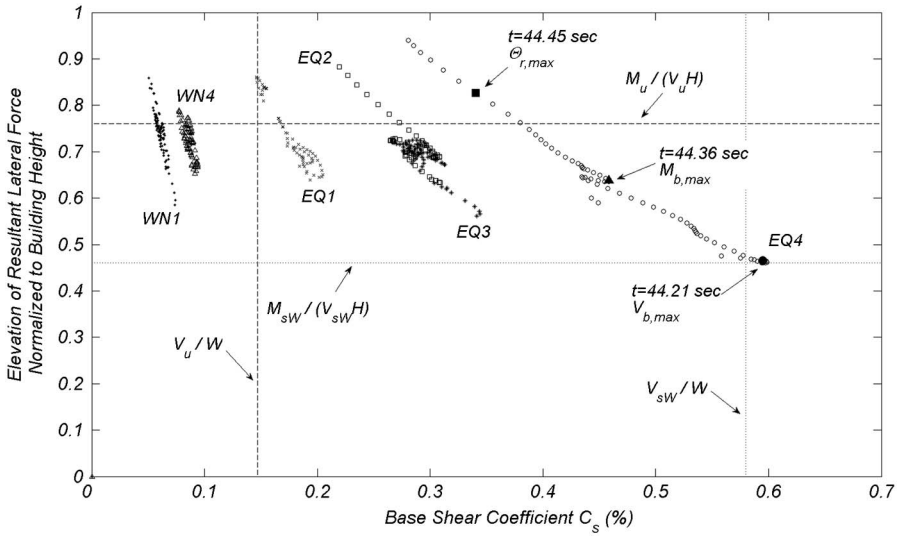

Fig. 11. Normalized effective height of resultant system seismic force versus base shear coefficient at instants for which $M_b > 0.9M_{b,\max}$

J. Struct. Eng. 2011.137:691-704.

little, with an average location at approximately 72% of the building height, thus implying a response largely dominated by the first mode. The same trend holds true for test EQ2. Test EQ3 showed a clear decrease in the height of the resultant lateral force because seismic input motion EQ3 was richer in high-frequency content than input motion EQ2 (see Fig. 1). In test EQ4, which showed significant nonlinear response, the location of the resultant lateral force varied considerably. At $t = 44.21$ s, this force was only at 46% of the building height and very close to the theoretical ratio $M_{sW}/(V_{sw}H)$. This explains the significant increase of the system total base shear force, while the system base overturning moment remained almost constant between 90 and 100% of its peak value. This observation clearly highlights the difference in magnitude between the moment and shear force overstrength factors Ω_{oM} and Ω_{oV}. The lowering of the location of the lateral force resultant occurred because of (1) the higher modes, especially second-mode

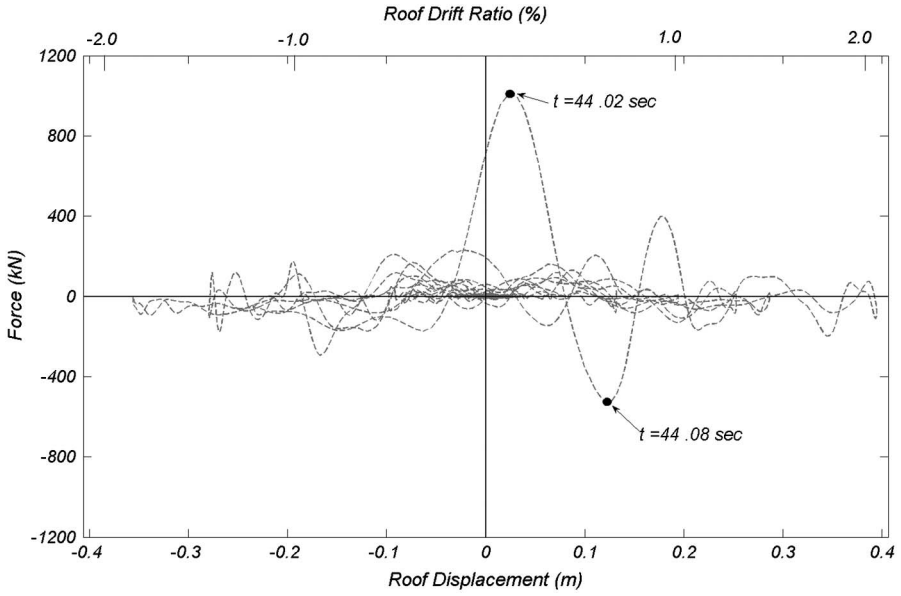

Fig. 12. Test EQ4—dynamic vertical force caused by motion of web wall and slabs versus roof displacement

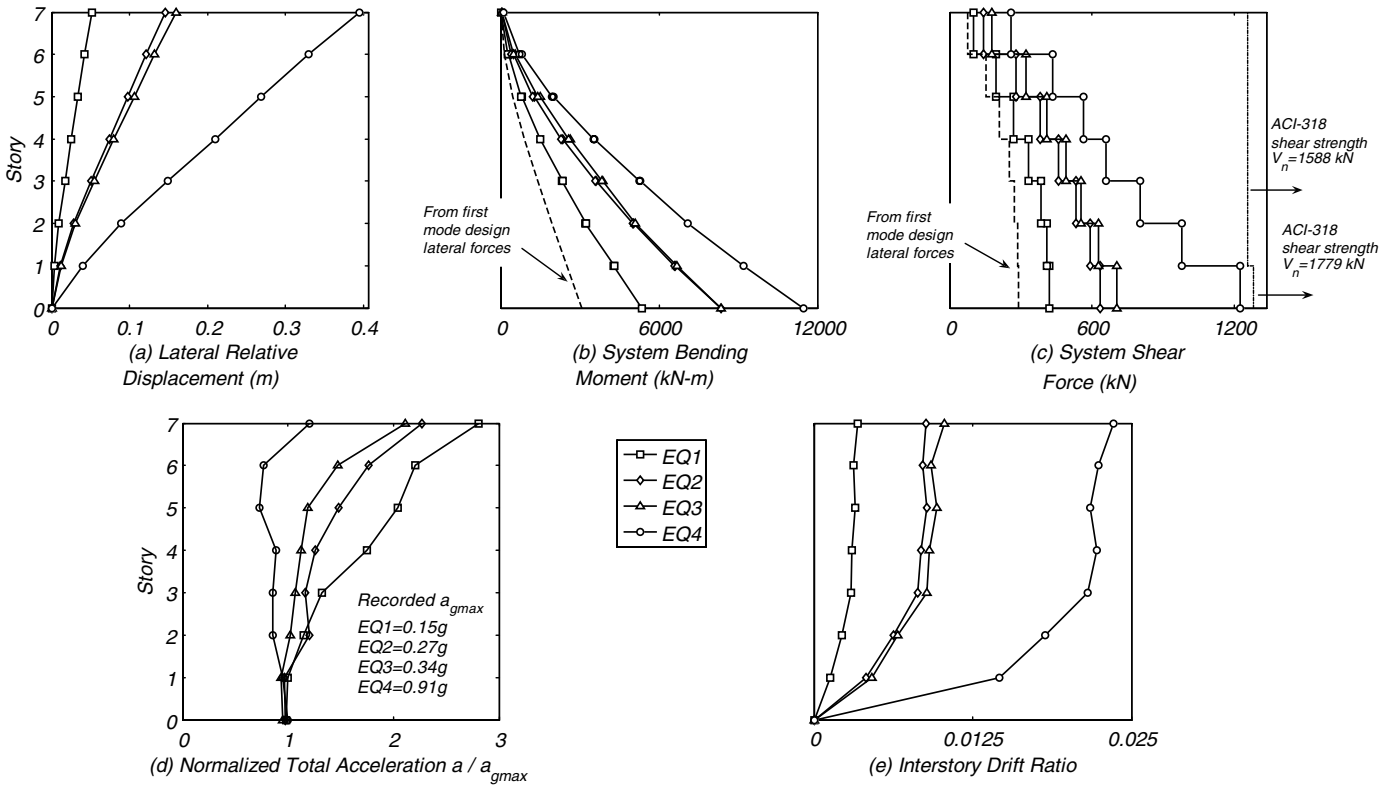

Fig. 13. Phase I—response envelopes

J. Struct. Eng. 2011.137:691-704.

contribution to the response; and (2) the coupling of the web and flange walls through the slabs (Panagiotou and Restrepo 2011). The system base shear force as well as the height of the resultant force accounting for kinematic system overstrength and second mode of response estimated with the displacement-based design method (Panagiotou and Restrepo 2011) is in excellent agreement with the corresponding measured values.

Vertical Acceleration Effects

Fig. 12 plots the dynamic vertical force resisted by the web wall and the gravity columns because of the vertical motion of the building versus roof displacement. This force was computed by using the measured vertical accelerations along the height of the building and tributary masses of the web wall and the slabs. Significant vertical accelerations and thus significant vertical inertia forces were measured between $t = 44.02$ and 44.08 s. These instants occur on the loading branch before the instant of maximum roof lateral relative displacement at $t = 44.45$ s (see also Fig. 5). The average vertical acceleration at $t = 44.02$ and 44.08 s was 0.82 and $-0.55g$, respectively. After this excursion, significantly smaller vertical accelerations were measured with peaks of less than an average of $0.2g$. The excursion of vertical accelerations occurring between $t = 44.02$ and 44.08 s is believed to be mainly caused by vertical motion of the table. The nonlinear deformations the web wall ends, which induced vertical motion in the slabs, also contributed to the vertical motion of the building.

Response Envelopes

Fig. 13 plots the envelopes of the main response quantities for tests EQ1–EQ4. Fig. 13(a) shows the lateral relative displacement envelope. With an increasing level of inelastic response, the development of a plastic hinge at the base resulted in concentration of curvature and rotation in this region and in almost a linear displacement profile from Levels 3 to 7. Figs. 13(b) and 13(c) show the envelopes of system bending moment and system total shear force, respectively. These plots also show the wall design shear force and design bending moment calculated from the first-mode design lateral forces obtained from the displacement-based design method used in this study. Fig. 13(c) also indicates the expected shear strength of the web wall calculated from ACI 318-05 [American Concrete Institute (ACI) Committee 318 2005] using measured material properties. Assuming that the entire back-calculated maximum base shear force V was resisted by the web wall with area A_w, the ratio V/A_w was equal to $0.27\sqrt{f'_c}$, where $f'_c = 37.9$ MPa. This value of shear stress is significantly smaller than $0.66\sqrt{f'_c}$ of Eq. 11.5.7.9 of ACI 318-05 (ACI Committee 318 2005), which corresponds to the upper bound of the probable shear strength provided from the shear reinforcement (V_s). The shape of the system shear force envelope in test EQ4 differs from the envelopes observed for tests EQ1–EQ3. The shear force envelope in test EQ4 has a nearly constant step per floor, whereas the shear force envelopes from the other tests are closer to that expected from a first-mode distribution of lateral forces, in which the magnitude of the steps are reduced from the top floor downward. The second-mode contribution to the response and the coupling of the web and flange walls through the slabs were responsible for the shape of the shear force envelope observed in test EQ4 (Panagiotou and Restrepo 2011).

Fig. 13(d) plots the envelopes of the total floor accelerations normalized by the peak table acceleration. For as long as the building showed limited inelastic response, that is, during tests EQ1–EQ3, floor accelerations were much greater than the table ground acceleration. This is consistent with the dynamic amplification expected from an elastic system. The roof amplification

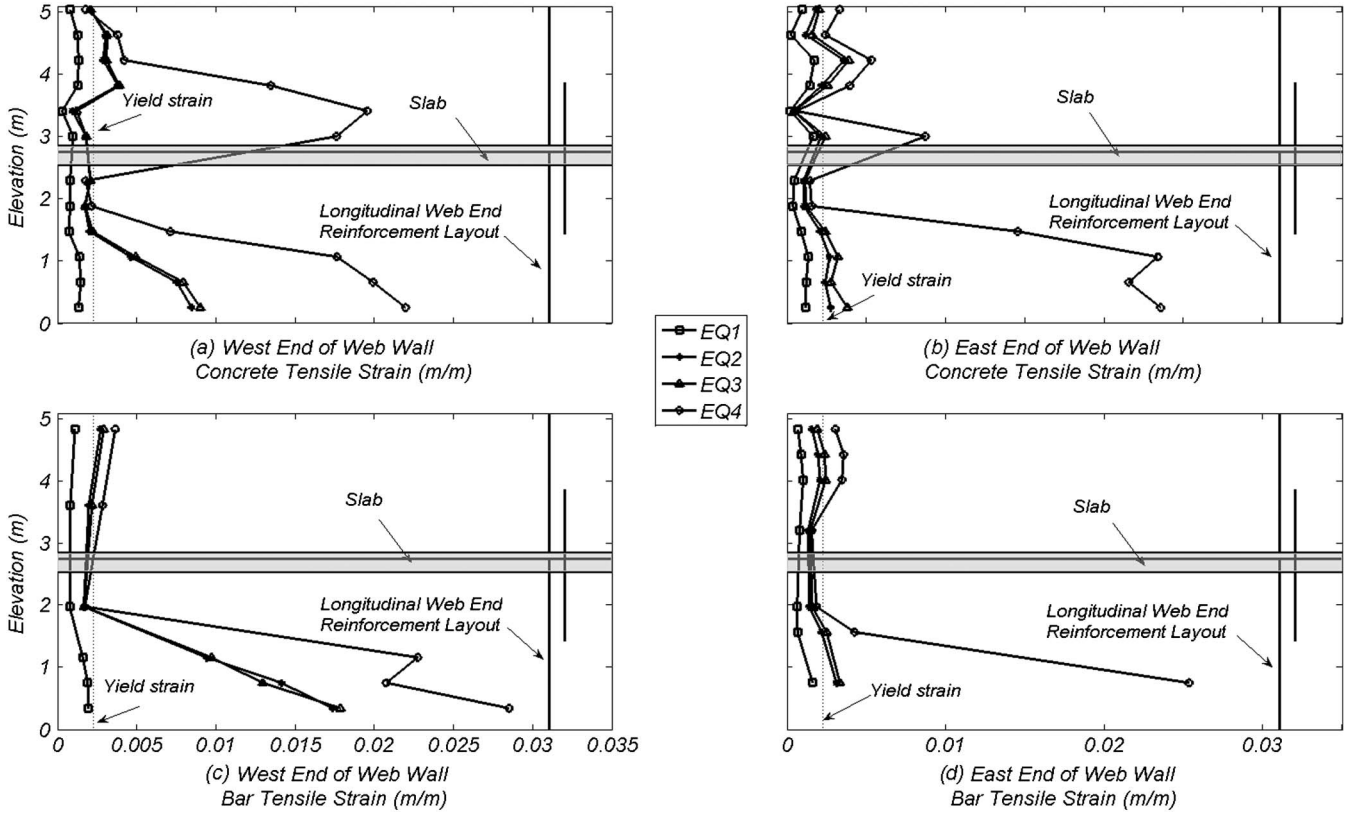

Fig. 14. Concrete and longitudinal reinforcement tensile strain envelopes

J. Struct. Eng. 2011.137:691-704.

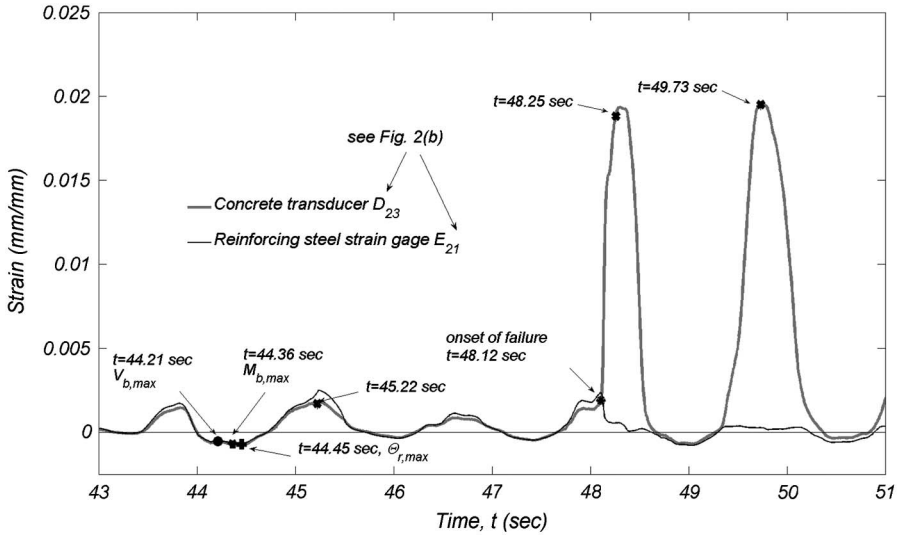

Fig. 15. Comparison of concrete surface and longitudinal reinforcement strains at Level 2 of west end of web wall during test EQ4

reached 2.9, 2.3, 2.1, and 1.2 in tests EQ1–EQ4, respectively. In test EQ4, when the building underwent significant nonlinear response, the peak total floor accelerations was close in magnitude to the peak table acceleration, indicating saturation of the response. This observation is consistent with the findings of Rodriguez et al. (2002). Fig. 13(e) displays the interstory drift ratio envelopes recorded during tests EQ1–EQ4. In all tests, interstory drift ratios increased in the first three levels and then remained nearly constant.

Strain Envelopes and Lap-Splice Response

Fig. 14 shows the concrete and rebar tensile strain envelopes at Levels 1 and 2 on the west and east ends of the web wall. Concrete strains were obtained from linear potentiometer measurements and are therefore average strains. Rebar strains were obtained from single strain gauges adhered to the bars. Except at the base of the wall, tensile strains on the concrete surface and in the rebar were of similar magnitude during tests EQ1–EQ3. In test EQ4, peak tensile strains in the concrete and steel were remarkably different at the top of the first-floor slab [compare Fig. 14(a) with Fig. 14(c) and Fig. 14(b) with Fig. 14(d)]. Such difference in strains is attributed to significant bar bond slip caused by deterioration of the lap splice, which was more pronounced in the westmost side of the web wall. During EQ4, a large vertical split crack occurred at the west lap-splice just above the first-floor slab [see Fig. 4(c)].

The lap-splice failure at the west end of the web wall occurred two cycles past the peak eastward displacement.

Fig. 15 plots the concrete and steel strain time histories in the lap splice from time $t = 43.0$–51.0 s. The times when $V_{b,\max}$, $M_{b,\max}$, and $\Theta_{r,\max}$ occurred are marked. The three instants when the three largest peak eastward displacement responses occurred ($t = 45.22$, 48.25, 49.73 s) as well as the onset of the lap-splice failure ($t = 48.12$ s) are also marked. The exact position of the displacement transducer D_{23} attached externally to the concrete and the strain gauge E_{21} attached to the reinforcing steel rebar are indicated in Fig. 2(b). The stains measured for the steel and the concrete are of similar magnitude even at the absolute maximum eastward displacement response at $t = 45.22$ s. After $t = 48.12$ s, the concrete tensile strain increased rapidly and greatly exceeded the steel tensile strain, indicating significant bond slip and eventually failure of the lap splice.

Conclusions

This paper describes the response of a 7-story load-bearing wall building built at full-scale during strong seismic tests conducted on the NEES-UCSD shake table. The building was designed for a site in Los Angeles following a displacement-based design procedure combined with capacity design for two hazard levels. The test addressed four issues relevant to construction optimization: (1) reduction in the longitudinal reinforcement; (2) use of a single curtain of reinforcement to transfer shear; (3) constrain of plasticity in the first level of the wall using capacity design; and (4) use of resistance-welded reinforcement in the boundary elements of the first level of the walls. The building was tested in a single direction parallel to the web wall under four historical earthquake records of southern California, including the strong intensity near-field motion recorded at the Sylmar station during the 1994 Northridge Earthquake. The response spectrum from the Sylmar motion matches closely that of the design basis earthquake calculated for the site. The level of performance of the building when subjected to the seismic input motions was found to be excellent overall. From the observed response of the building, the following conclusions can be drawn:

1. In the seismic tests of the building, all the performance objectives selected for immediate occupancy and life-safety were met.
2. Three-dimensional interaction effects between the web wall, flange wall, and the slabs—referred to here as kinematic overstrength—caused significant increase in the system overturning moment capacity as well as of the shear force demand in the web wall. To a specific extent, this was attributable to the characteristics of the test structure. Given the undesirable consequences of shear failures in reinforced concrete buildings, such shear force demands that are larger than expected should be accounted for in design.
3. Dynamic effects (higher-mode effects) observed in the response of the building system can augment the shear force demand in individual walls and significantly increase the total accelerations along the height of the building.
4. The experimental response largely verified the displacement-based analysis procedure proposed in the companion paper (Panagiotou and Restrepo 2011), including the way in which

J. Struct. Eng. 2011.137:691-704.

the effects of kinematic system overstrength and the second mode of response were accounted for.

5. Lap splices should be avoided in at least twice the depth of a wall from the critical region at which a plastic hinge will develop, as is currently recommended in codes of practice. Also, other means of providing bar splicing should be considered or developed near plastic hinges.
6. Resistance-welded grids acting as transverse reinforcement in the boundary elements of walls provided excellent stability for the longitudinal reinforcing bars after spalling of the concrete cover.
7. The elongation of the tension chord in reinforced concrete walls may induce large tensile and compressive forces in gravity columns located near such walls. These forces cannot be quantified from routine first-order analysis. Simple sketches displaying the deformed shape of the lateral force–resisting elements can highlight the need to specially detail some of these gravity load–resisting elements.
8. A single curtain of transverse reinforcement was successfully used in the test building for unidirectional excitation. The use of such detail resulted in an accelerated construction schedule. The adequacy of a single curtain of reinforcement should be verified for the case of bidirectional excitation.

Acknowledgments

The authors sincerely thank the Englekirk Board of Advisors, a University of California, San Diego industry group supporting research in structural engineering. They specially thank Dr. Robert Englekirk for his support and advice. They also thank the Charles Pankow Foundation and the Portland Cement Association, who provided financial support in reducing the data acquired in this project. Thanks also to Ms. Santina Watts, who helped in the preparation of drawings, and to Ms. Isabel Campos, who helped with the development of instrumentation.

Notation

The following symbols are used in this paper:

A_w = web-wall cross section;
a = total floor acceleration;
a_g = ground acceleration;
$a_{g,\max}$ = peak table acceleration;
C_S = base shear coefficient;
f'_c = concrete compressive strength;
H = total building height;
l_w = length of web wall;
$M_{b,\max}$ = maximum system base moment;
$M_{f\mathrm{E}}$ = moment capacity of east end of slotted connection;
$M_{f\mathrm{W}}$ = moment capacity of west end of slotted connection;
$M_{s\mathrm{E}}$ = theoretical maximum system base bending moment for eastward response;
$M_{s\mathrm{W}}$ = theoretical maximum system base bending moment for westward response;
M_u = design moment;
N = axial force in web wall;
N_f = axial force in web wall due to slotted slab connection;
R = response modification factor;
S_a = spectral acceleration;
S_d = spectral displacement;
s_h = distance between confinement grids;
T = fundamental period of building;
T_2 = second-mode period of building;
t = time (s);
V = shear force;
V_b = base shear force;
$V_{b,\max}$ = maximum system base shear force;
V_f = shear force of slotted slab connection;
V_p = web-wall probable shear strength;
V_s = shear strength provided from shear reinforcement;
$V_{s\mathrm{E}}$ = theoretical maximum system base shear force for eastward response;
$V_{s\mathrm{W}}$ = theoretical maximum system base shear force for westward response;
V_u = design shear force;
$v_{g,\max}$ = peak ground velocity;
W = total seismic weight excluding foundation weight;
γ = normalized height of position of resultant lateral force;
ε_s = reinforcing steel strain;
ε_y = reinforcing steel yield strain;
$\Theta_{r,\max}$ = maximum roof drift ratio;
μ_φ = curvature ductility;
φ_y = reference yield curvature;
Ω_{oM} = system moment overstrength;
Ω_{os} = section flexural overstrength; and
Ω_{oV} = system shear overstrength.

References

American Concrete Institute (ACI) Committee 318. (2005). "Building code requirements for structural concrete and commentary." *ACI 318-05*, Farmington Hills, MI.

ASCE. (2006). "Minimum design loads for buildings and other structures." *ASCE/SEI 7-05*, Reston, VA.

Bock, Y., Panagiotou, M., Yang, F., Restrepo, J., and Conte, J. (2006). "Shake table tests of a full scale reinforced concrete wall building: Real time 50 Hz GPS displacement measurements." *Proc., 8th National Conf. on Earthquake Engineering*, Earthquake Engineering Research Institute, Oakland, CA.

Matlab reference guide. (2008). The MathWorks, Inc., Natick, MA.

Moaveni, B., He, X., Conte, J. P., and Restrepo, J. I. (2010). "Damage identification study of a seven-story full-scale building slice tested on the UCSD-NEES shake table." *Struct. Saf.*, 32(5), 347–356.

Moaveni, B., He, X., Conte, J. P., Restrepo, J. I., and Panagiotou, M. (2011). "System identification study of a 7-story full-scale building slice tested on the UCSD-NEES shake table." *J. Struct. Eng.*, 137 (6), 705–717.

Ozcelik, O., Luco, J. E., Conte, J. P., Trombetti, T. L., and Restrepo, J. I. (2008). "Experimental characterization, modeling and identification of the NEES-UCSD shake table mechanical system." *Earthquake Eng. Struct. Dyn.*, 37(2), 243–264.

Panagiotou, M. (2008). "Seismic design, testing and analysis of reinforced concrete wall buildings." Ph.D. thesis, Dept. of Structural Engineering, Univ. of California, San Diego, La Jolla, CA.

Panagiotou, M., and Restrepo, J. I. (2007). "Design and computational model for the UCSD 7-story structural wall building slice." *SSRP 07-09 Rep.*, Dept. of Structural Engineering, Univ. of California, San Diego, La Jolla, CA.

Panagiotou, M., and Restrepo, J. I. (2011). "Displacement-based method of analysis for regular reinforced-concrete wall buildings: Application to a full-scale 7-story building slice tested at UC–San Diego." *J. Struct. Eng.*, 137(6), 677–690.

Panagiotou, M., Restrepo, J. I., and Conte, J. P. (2007). "Shake table test of a 7-story full scale reinforced concrete structural wall building slice. Phase II: T-wall." *SSRP 07-08 Rep.*, Dept. of Structural Engineering, Univ. of California, San Diego, La Jolla, CA.

J. Struct. Eng. 2011.137:691-704.

Park, R., and Paulay, T. (1975). *Reinforced concrete structures*, Wiley, Hoboken, NJ.
Paulay, T., and Priestley, M. J. N. (1992). *Seismic design of reinforced concrete and masonry buildings*, Wiley, Hoboken, NJ.
Restrepo-Posada, J. I., Dodd, L. L., Park, R., and Cooke, N. (1994). "Variables affecting cyclic behavior of reinforcing steel." *J. Struct. Eng.*, 120(11), 3178–3196.
Rodriguez, M. E., Restrepo, J. I., and Carr, A. J. (2002). "Earthquake-induced floor horizontal accelerations in buildings." *Earthquake Eng. Struct. Dyn.*, 31(3), 693–718.
Van Den Einde, L., et al. (2004). "Development of the George E. Brown Jr. Network For Earthquake Engineering Simulation (NEES) Large High Performance Outdoor Shake Table at the University of California, San Diego." *Proc., 13th World Conf. in Earthquake Engineering*, International Association for Earthquake Engineering (IAEE), Tokyo, Paper No. 3281.
Wood, S. (1991). "Performance of reinforced concrete buildings during the 1985 Chile earthquake: Implications for the design of structural walls." *Earthquake Spectra*, 7(4), 607–638.